We are IntechOpen,
the world's leading publisher of
Open Access books
Built by scientists, for scientists

6,900
Open access books available

186,000
International authors and editors

200M
Downloads

154
Countries delivered to

Our authors are among the

TOP 1%
most cited scientists

12.2%
Contributors from top 500 universities

CLARIVATE ANALYTICS

BOOK CITATION INDEX

INDEXED

WEB OF SCIENCE™

Selection of our books indexed in the Book Citation Index
in Web of Science™ Core Collection (BKCI)

Interested in publishing with us?
Contact book.department@intechopen.com

Numbers displayed above are based on latest data collected.
For more information visit www.intechopen.com

Weathered Granite Soils

Xirong Niu

Abstract

A great deal of weathered granite soils are distributed in mountainous areas around the world. With further improvements to the civil engineering, more and more construction infrastructures (roads, railways, dams, etc.) in mountainous areas will be built. Making full use of weathered granite soils, a type of special geomaterial, can alleviate the shortage of building materials in mountainous areas. Weathered granite soil has its own unique physical and mechanical properties, e.g., disintegrative, easy weathering, and particle breakage. In this chapter, a large number of field investigations and laboratory tests (including X-ray diffraction, sieving, heavy compaction, and large-scale triaxial) have been carried out. The process of weathering, the influence factors on particle breakage, and the mechanical properties of compacted weathered granite have been discussed. The results show that particle gradation, mineral content, blows per layer, and stress level have a significant effect on the particle breakage characteristics of weathered granite soils. The experimental results show that the product of the stress ratio at shear failure M_f and the stress ratio at characteristic state point M_c is not a constant but a power function of an average main stress p due to particle breakage. Hereby, the constitutive model of weathered granite soils was proposed.

Keywords: weathered granite soils, weathering mechanism, particle breakage, mechanical behavior, modified strength condition, constitutive model

1. Introduction

As a member of igneous rock family, granite is formed by magma inside the Earth. The main components of igneous rocks are quartz, feldspar, mica, and hornblende [1]. The features of granite include the full crystal-grain structure, hard texture and uniform material, and high compressive strength (120–200 MPa). Because joints exist in feldspar and mica, there are three groups of primary joints in granite. The significant difference (nearly doubled) between the expansion coefficients of quartz and feldspar causes granite surface to crack easily in the process of expansion and contraction. Hence, granite would weather easily, especially the one with coarse grain structure [2]. During the weathering process, granite is also influenced by long-term, geological tectonic movement, and climate changes in the specific geographical environment. Based on the different physical and chemical properties of granite mineral composition and the different degrees of weathering of granite, decomposed granitic soils are generally classified as weak weathering, weathering, strong weathering, and residual [3].

With further improvements to the civil infrastructure, more and more engineering construction projects (roads, railways, dams, etc.) will be built in complex mountainous areas. However, the shortage of building materials is an acute problem

during constructing these infrastructures in mountainous areas. It is very important to study the engineering properties and applicability of special materials, e.g., weathered granite soil, in mountain area to solve the problem of shortage of building materials. Besides nonlinear stress-strain, elastic-plastic, dilatancy (shrinkage), and other properties, easy weathering and particle breakage are the distinctive and unique engineering property of weathered granite. The particle size distribution of the in situ soils is controlled by weathering process. Furthermore, the particle breakage characteristics of soils are affected by the particle size distribution. The particle size distribution of in situ weathered granite soil has been paid little attention in previous studies, but it is very important to have a full understanding of the particle size distribution of in situ weathered granite soil, because the particle size distribution has considerable influences upon engineering properties of weathered granite soil such as compatibilities, permeabilities, and strength-deformation characteristics [4–7].

In this chapter, the weathering mechanism, particle breakage, mechanical properties (including compaction characteristic, bearing characteristics, strength characteristics, and shearing-dilatancy characteristics), and constitutive model of weathered granite soils from Shanxi, China, were investigated. The results can provide a basis for the comprehensive understanding of the engineering characteristics of weathered granite soils and references for the utilization of weathered granite soils in engineering practice.

2. Specimen preparation and test methods

The weathered granite soil samples used in this chapter were obtained from a site near Mount Yunzhong (shown in **Figure 1**), a branch of the Lu-liang Mountains, on the eastern outskirts of Xinzhou City, Shanxi Province, China. The weathered granite soil was used as a part of the subgrade materials in the Xinbao highway (Xinzhou City to Baode City). There were three colors of the weathered granite in the field, red-brown, yellow-brown, and gray, as shown in **Figure 1**. The in situ dry unit weight and moisture content of the weathered granite were 17.82–18.22 kN/m^3 and 4.9–5.5%, respectively.

The excavation range of the filling materials used for Xinbao highway (Shanxi Province, China) was mined at a depth of less than 30 m on average under the

Figure 1.
Photograph of weathered granite samples.

surface of the Lu-liang Mountains. This is a general practice in producing subgrade materials for highways. Because the red-brown and the yellow-brown weathered granites were located at depths of less than 30 m, the lab tests in this chapter are focused on these two kinds of samples. The embankment is mainly filled with red-brown weathered granite, so parts of the tests in this chapter were mainly aimed at red-brown samples.

Because the physical meaning of Fukumoto's weathering model [4] is clear and easy to use, this model was used in this chapter to evaluate the weathering process of granite. After the thorough investigation on the distribution of in situ weathered granite, numerous sieving tests on a large number of granite samples obtained from typical sections A and B (shown in **Figure 2**) were carried out. According to Fukumoto's grading model, geological year's parameter m and geometric progression constants r of granite samples at different depths were calculated. The experimental tests involved in this chapter, including X-ray diffraction, sieving, heavy compaction [8], and large-scale triaxial test [9], were investigated to research the particle breakage characteristics of compacted weathered granite.

Figure 3 shows the composition of the rock samples in this study. **Figure 3** shows that the colors of the samples became gradually brighter with an increase in the quartz content. The increase in potassium feldspar or feldspar content was the

(a) **(b)**

Figure 2.
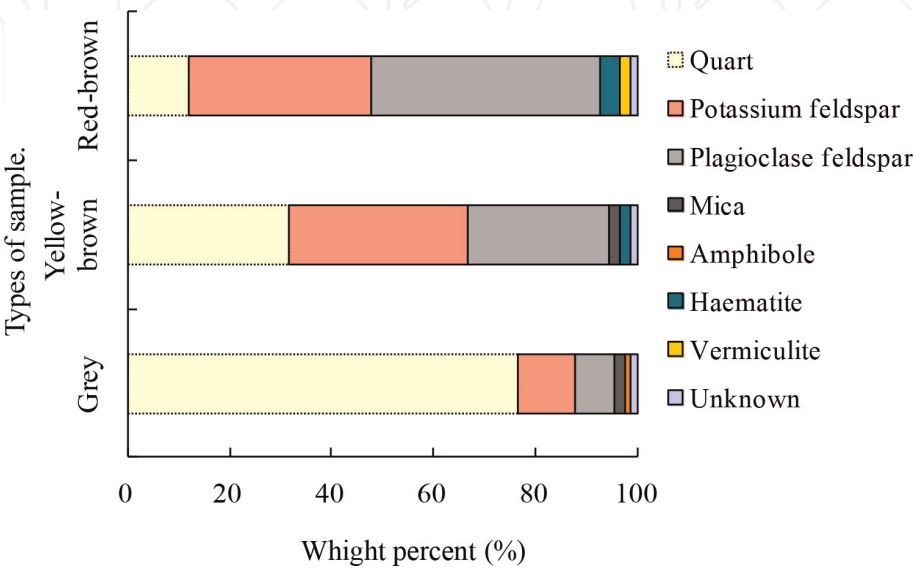*Photograph of field sampling: (a) section A and (b) section B.*

Figure 3.
Mineral composition of weathered granite samples.

main cause of the brighter colors of the rocks. Geng et al. [10] noted that the amphibole was bluish-green, and the biotite was yellow in Mount Yunzhong. In addition, Geng et al. [10] described the main body of the granite as a coarse grain (porphyritic granite), with fine-grained granite on the edge. The three types of samples used in this chapter had quartz (mean 40.3%) and feldspar (mean 54.3%) as the dominant minerals present with smaller amounts of mica (mean 1.3%), amphibole (mean 2%), hematite (0.5%), vermiculite (1%), and unknown (1%) materials.

3. Weathering process

Based on the geometric fractal theories and some assumptions, Fukumoto [4] proposed a gradation equation for decomposed granite soils by using mathematical statistics method and made it possible to quantificationally describe the weathering process of granite by using a certain mathematical model to evaluate the particle breakage of weathered rock. Because Fukumoto's model is more scientific and easier to use, this model has been widely used in describing the process of rock weathering. Thus, this model was also used in this chapter to describe the weathering process of in situ weathered granite.

Figure 4 shows changes of parameters m and r for the samples at different depths of mountain profile, h.

The results of statistical analysis indicate an approximate power function relationship between h and m (or r), and the correlation of relationship was relatively good. The power function relationships between h and m (or r) in section A are shown as follows:

$$m_A = 3.324h^{-0.706} \tag{1}$$

$$r_A = 0.243h^{0.153} \tag{2}$$

where h is the depth of granite samples, which was measured from the surface of mount, m_A is the geological year's parameter in section A, and r_A is the geometric progression constant in section A.

The power function relationships between h and m (or r) in section B are shown as follows:
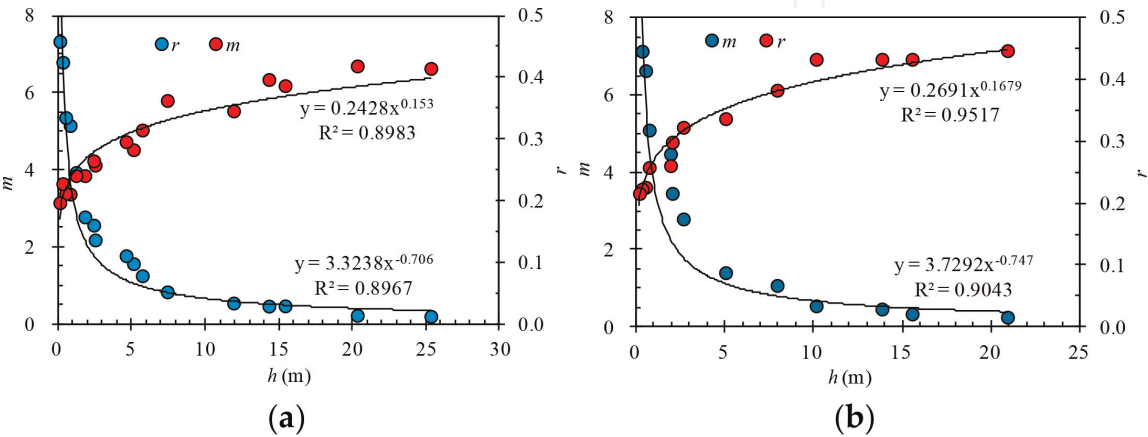
$$m_B = 3.729h^{-0.747} \tag{3}$$

Figure 4.
Change of parameters m and r for samples at different depths: (a) section A and (b) section B.

$$r_{\mathrm{B}} = 0.269 h^{0.168} \tag{4}$$

where m_{B} is the geological year's parameter in section B and r_{B} is the geometric progression constant in section B.

Actually, the geological year's parameter, m, reflects the degree of geological actions (including physical actions and chemical actions) [11]. The deeper the granite is buried, the less the geological action will affect it. The above results indicate that m was close to zero at a depth of 20–25 m under the surface of the mount in sections A and B, which indicate that the physical and chemical actions on the granite in this research can be negligible at this depth. The geometric progression constant, r, represents the integrality of rock. The r of section A and section B studied in this chapter was close to a certain value at a depth of 25 and 20 m, respectively, which indicates that the granite in Mount Yunzhong was close to the complete unweathered state at a depth of 20–25 m.

It can be found from the results that the m of section A was larger than that of section B at the same depth, indicating that the ability of section A to resist geological and climatic environment was worse than that of section B. On the other hand, the r of section A was smaller than that of section B at the same depth, which illustrates that the integrality of granite in section A was worse than that in section B [11]. Although section A and section B are under the same geological and climatic environment, the values of m (or r) are different between these two sections. The main reason for the difference was the difference in internal properties (e.g., the mineral composition of rocks) of weathered granite between these two sections. Of course, some external factors could not be excluded; for example, the probability of fracture distribution of section A is larger than that of section B.

4. Particle breakage characteristics

Many aspects, such as particle gradation, mineral composition, blows per layer, and stress level, can influence the characteristics of particle breakage of compacted weathered granite.

Hardin [12] proposed the concept of relative breakage (B_{r}), which was achieved from the variation in particle size distribution curves before and after loading. Relative breakage can embody the overall change in particle size distribution before and after loading and overcomes the shortcoming of using single index of sieving test results (percentage of particles passing a given sieve size or sieve size corresponding to a given percentage passing) as the evaluation index for particle breakage [13–16]. In view of the above, B_{r} has been widely used in evaluating soil particle breakage characteristics, because it can represent the basic attribute of the soil material and is more scientific and reasonable to use.

4.1 Particle gradation

Standard heavy compaction tests on four red-brown samples and four gray samples of weathered granite with different gradations under optimum moisture content conditions were investigated. Sieving tests were implemented on the samples before and after compaction, and the uniformity coefficient ($C_{\mathrm{u}} = d_{60}/d_{10}$) and relative breakage (B_{r}) of the samples before and after the compaction test were calculated. The relationship between C_{u} and B_{r} is shown in **Figure 5** [11]. The test results show that B_{r} decreased with the increase of C_{u} which indicates that as the C_{u} of weathered granite increased, the degree of particle breakage was reduced because of the enhancement of the intergranular locking effect. In addition, it can be seen
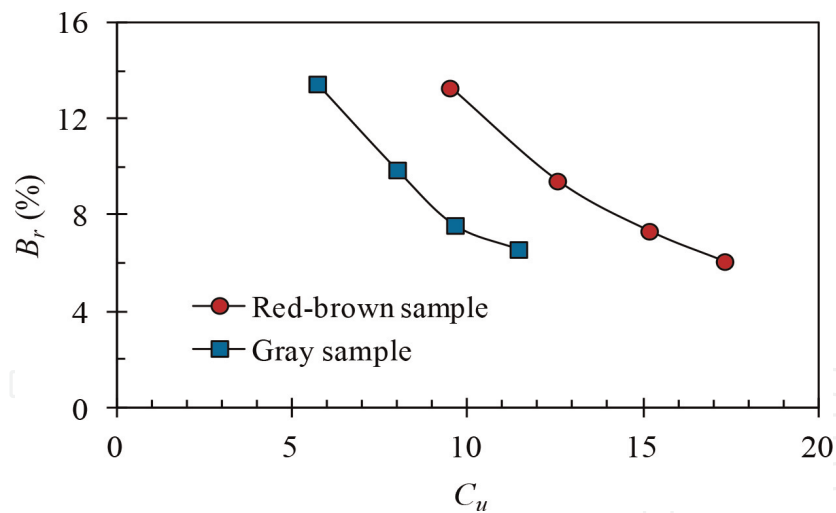
Figure 5.
B_r-C_u curves.

that the rate of decrease of relative breakage of the red-brown sample was higher than that of the gray sample, reflecting that because the degree of weathering of red-brown weathered granite is higher than that of gray weathered granite, the strength of the red-brown sample was less than that of the gray sample. This shows that the sensitivity of the red-brown sample to particle heterogeneity was greater than that of the gray sample [11].

4.2 Mineral content

The red-brown, yellow-brown, and gray weathered granite samples were prepared with approximately the same particle size distribution. Standard heavy compaction tests were performed on the samples under optimum moisture content conditions [11]. The results of sieving before and after the test are shown in **Figure 6**.

The relationship between relative breakage and quartz (or feldspar) content was analyzed by calculating the relative breakage of different samples before and after
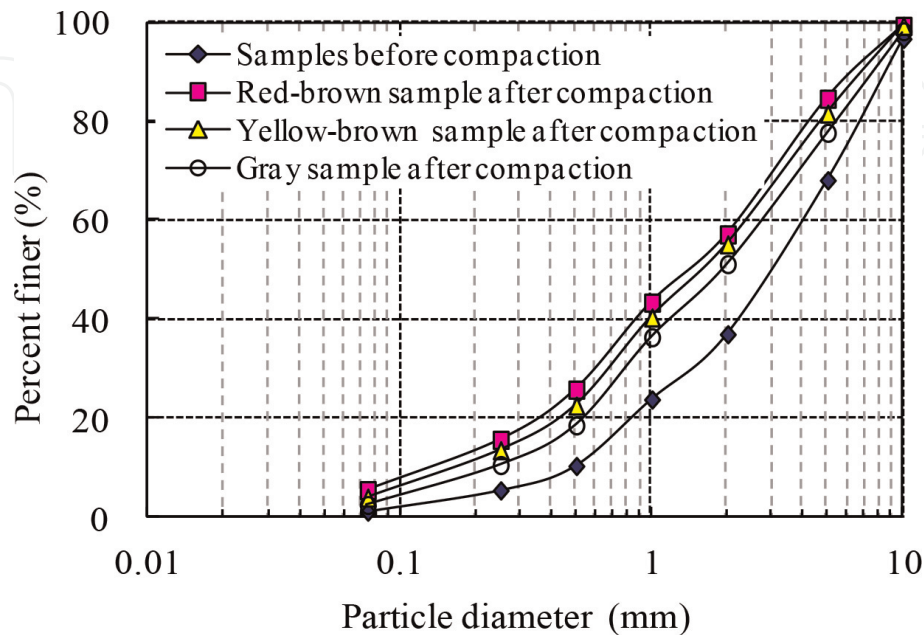

Figure 6.
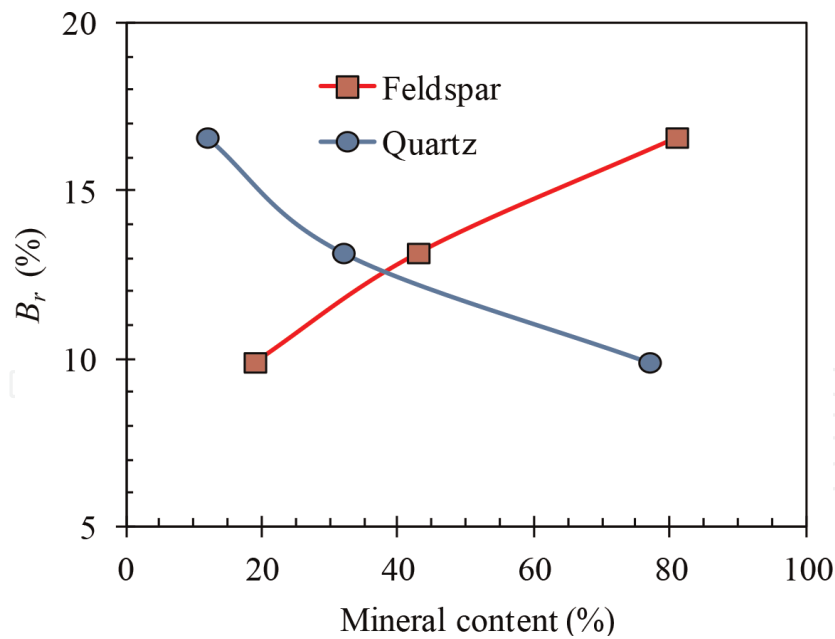*Sieving curves of different samples before and after the test.*

Figure 7.
Relationship curve between mineral content and B_r.

the standard compaction test. **Figure 7** shows the relationship between relative breakage and quartz (or feldspar) content. It can be seen from the figures that B_r decreased with the increase of quartz content, while B_r increased with the increase of feldspar (=plagioclase feldspar + potassium feldspar). The results show that quartz and feldspar content have an obvious effect on the particle breakage characteristics of weathered granite [11].

The main reasons that the B_r of samples with high quartz content after compaction test was small are as follows: (1) the probability of breakage of samples with more quartz content is small because quartz has a high strength, (2) samples with high quartz content have strong ability to resist being weathered, and (3) there are few microcracks in samples with high quartz content. On the contrary, feldspar has little strength and is easily weathered, so the samples with higher feldspar content showed obvious particle breakage characteristics [11].

4.3 Blows per layer (compaction degree)

In order to analyze the effect of blows per layer of samples on the particle breakage properties of weathered granite, four red-brown weathered granite samples with the same initial particle size distribution were prepared, and four different heavy compaction tests were conducted, with blows per layer (BPL) of 30, 50, 75, and 98 [11]. The sieving results before and after the tests are shown in **Figure 8**.

As shown in **Figure 9**, the relative breakage increased with an increase in blows per layer, but the increasing level of relative breakage decreased. Furthermore, with the further increase of blows, B_r tended toward a certain limit value. Considering the engineering practice, the compaction degree of samples was analyzed, and the compaction degrees of samples and corresponding relative breakage are depicted in **Figure 10**. It can be concluded from this figure that there is an approximate linear growth relationship between compaction degree and B_r. It can be found that for the same weathered granite fillings, relative breakage can be used to reflect the compaction performance indirectly on the basis of the relationship between compaction effect and compaction performance. Excessive compaction may lead to excessive particle breakage of soils and is not conducive to the long-term stability of subgrade [11].
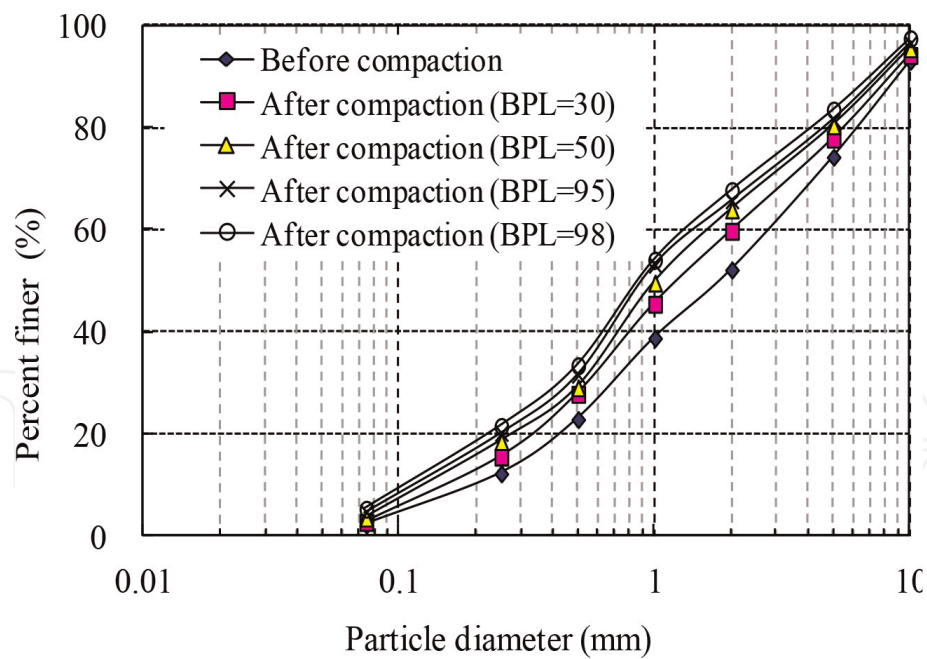
Figure 8.
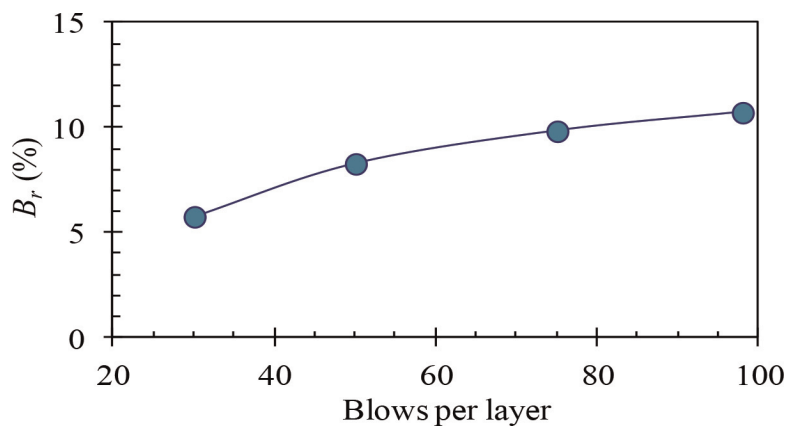*Sieving curves of samples under different blows per layer. BPL: blows per layer.*

Figure 9.
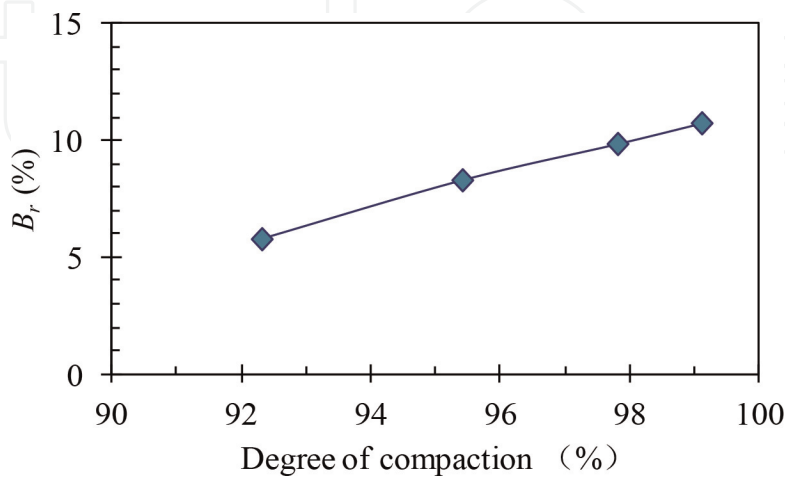*Relationship curve between blows per layer and B_r.*

Figure 10.
Relationship curve between degree of compaction and B_r.

4.4 Stress level

The breakage of soil particles in a sample of rockfill under moderate stress will be quite evident [11]. For the purpose of studying the particle breakage

characteristics of compacted weathered granite soil under different stress levels, particle size analysis tests were conducted on the samples before and after consolidated drained large-scale triaxial tests, and the relationship between relative breakage and confining pressure (or stress ratio, q/p) was analyzed [11].

Because specimens for the triaxial test must be prepared by the vibrating forming method, particles of the specimens may be partially crushed. In order to improve the accuracy of the experiment, two specimens for the large-scale triaxial test under the same confining pressure were artificially prepared with approximately the same particle size distribution before vibrating compaction. One of the samples was sieved after vibrating compaction and before the triaxial test. The results of the sieving test for this sample were used as the initial gradation of the other sample for the triaxial test [11].

From the stress-strain curve of samples in this study, it can be seen that when the axial strain reached 15%, the residual strength of the specimen under different confining pressures reached its constant value. Therefore, when the axial strain reached 15%, the triaxial tests were forced to stop, and then the sieving tests were performed. **Figures 11** and **12**, respectively, show variations in relative breakage (B_r) with confining pressure (σ_3) and stress ratio (q/p) [11].

As indicated in **Figure 11**, at the end of the triaxial test, the relative breakage of samples increased with the increase of confining pressure, while the increasing amplitude of relative breakage decreased slightly with the increase of confining
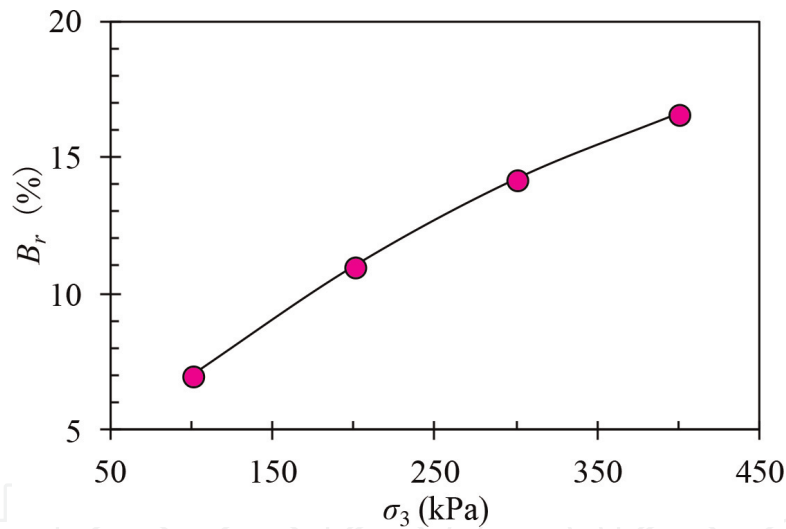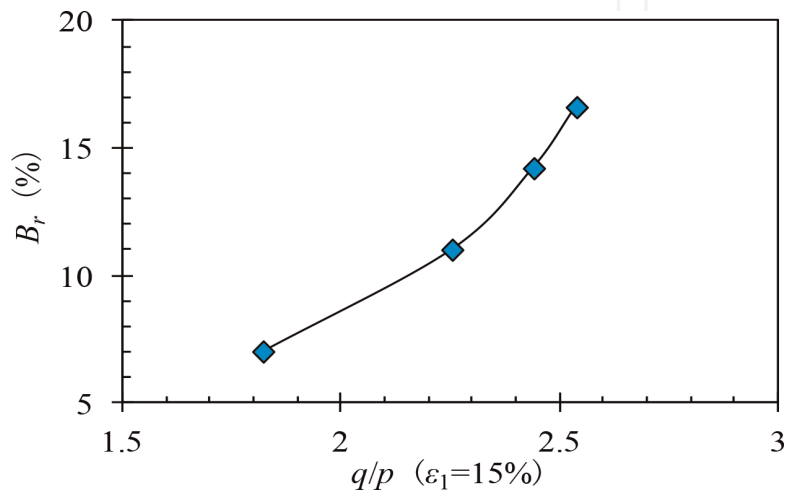

Figure 11.
B_r-σ_3 curves.

Figure 12.
B_r-q/p ($\varepsilon_1 = 15\%$) curves.

pressure. It can be considered that the higher confining pressure limited the further compaction and movement of soil particles in soil samples and resulted in producing microcracks and fracture within a single particle. The data in **Figure 12** illustrate that at the end of the experiment ($\varepsilon_1 = 15\%$), both relative breakage B_r and the amplitude of B_r increased with the increase of the stress ratio q/p. These results indicate that under the same axial strain conditions, more particles were broken due to the increased strain confinement caused by higher confining pressure [11].

5. Mechanical behavior

5.1 Compaction characteristics

Figure 13 shows the compaction curves for the red-brown and yellow-brown samples with different clay contents. It can be seen from **Figure 13** that the peak maximum dry density (MDD) values occur most significantly when the clay contents are in the range of 7.5–10%. The peak MDD of the red-brown and the yellow-brown samples of weathered granite soil is 2.32 and 2.38 g/cm³, respectively. The results of the tests clearly show that as the clay content increases, the MDD tends to be considerably reduced after it reaches the peak MDD. Therefore, the experimental results show that the clay content of weathered granite soil has a remarkable influence on its compaction characteristics. Furthermore, at peak MDDs, the clay content of red-brown weathered granite soil is 1% larger than that of yellow-brown weathered granite soil. Because the particles of the red-brown samples were smaller than the ones in the yellow-brown samples, the yellow-brown samples mixed with clay could be easily formed into the suspended-dense structures in the process of compaction. The red-brown samples mixed with clay could be easily formed into the skeleton-dense structures. Consequently, the peak MDD of red-brown samples was smaller than that of yellow-brown samples. In addition, the higher the clay content, the larger is the optimum moisture content, and this relationship is approximately linear. These results also indicate that because the gradation of red-brown samples is finer than yellow-brown, the optimum moisture content (OMC) of red-brown samples is 0.1% smaller than yellow-brown. It is noted that the
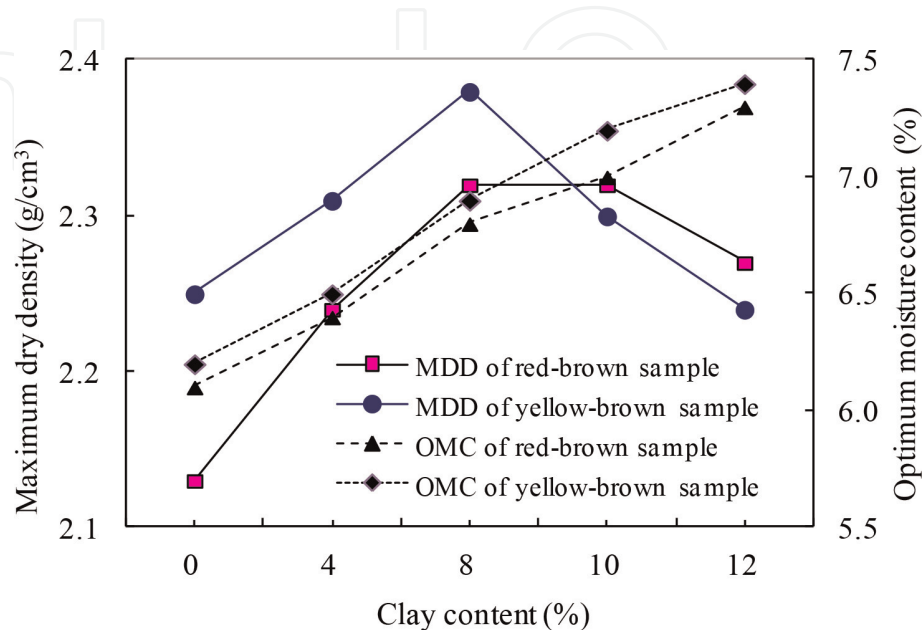

Figure 13.
Compaction curves for weathered granite samples with differing clay content.

increase of OMC slowed down slightly when the clay contents of the samples were more than 8% [17].

5.2 Bearing characteristics

Figure 14 represents the relationship of clay contents and CBR (California Bearing Ratio) obtained from different compaction tests, with the blows per layer of 30, 50, and 98, respectively. As shown in **Figure 14**, the CBR comes to a peak value when the value of blows per layer is 50 or 98. Because the compaction power is not enough to make rock material in a dense state when compacted under 30 blows, the CBRs of the samples with 30 blows do not arise to a peak value. However, with the increase of clay content ratio, the samples with 30 blows will eventually arise to a peak CBR. The experimental results show that the peak value of CBR increases with the increase of blows per layer. But the results also show that as the blows per layer increase, the clay content ratio at the point of peak CBR decreases. It is noted that the clay content ratio at the point of peak CBR with 98 blows per layer is approximately 4%, which is 4% less than the clay content ratio at the point of peak maximum dry density. The cause of the above results is mainly because that when clay content ratio exceeds a certain value (i.e., 4%), the interlocking structure of the compacted weathered-granite would be opened by the clay in the material, the internal friction angle (φ) would be decreased, and the penetration resistance subsequently would be declined. Finally, the clay content ratio at the point of peak CBR is larger than that the ratio at the point of peak maximum dry density [17].

5.3 Strength characteristics

Figure 15 shows the typical stress-strain relationship of the CD tests on four representative red-brown samples of pure weathered soil under four different confining pressures, where σ_1 is the axial stress, σ_3 is the confining pressure, and $d\varepsilon_1$ is the axial strain. **Figure 16** shows this typical ε_v-ε_1 relationship of the CD tests, where ε_v is the volumetric strain.

It can be found in **Figure 15** that the peak deviator stress increases as the confining pressure increases. The internal particles of weathered granite soil could be overturned, stridden, and dislocated under lower confining pressure and could
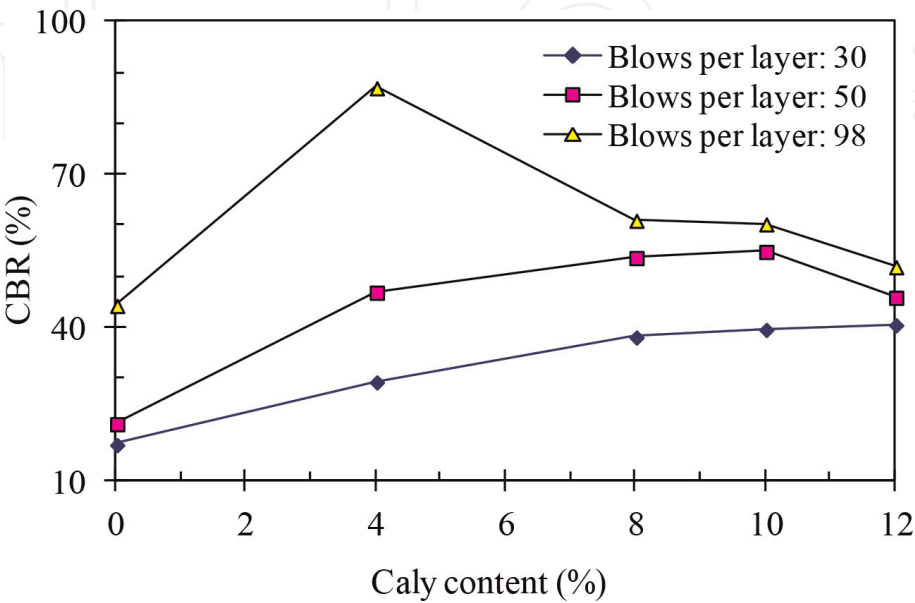
Figure 14.
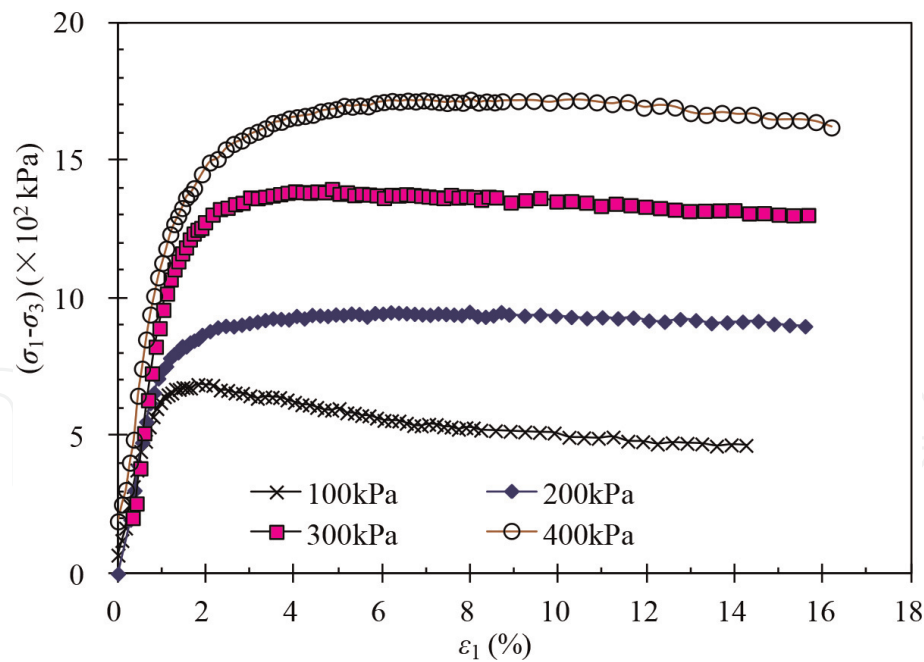*Change in CBR for soils with differing clay content.*
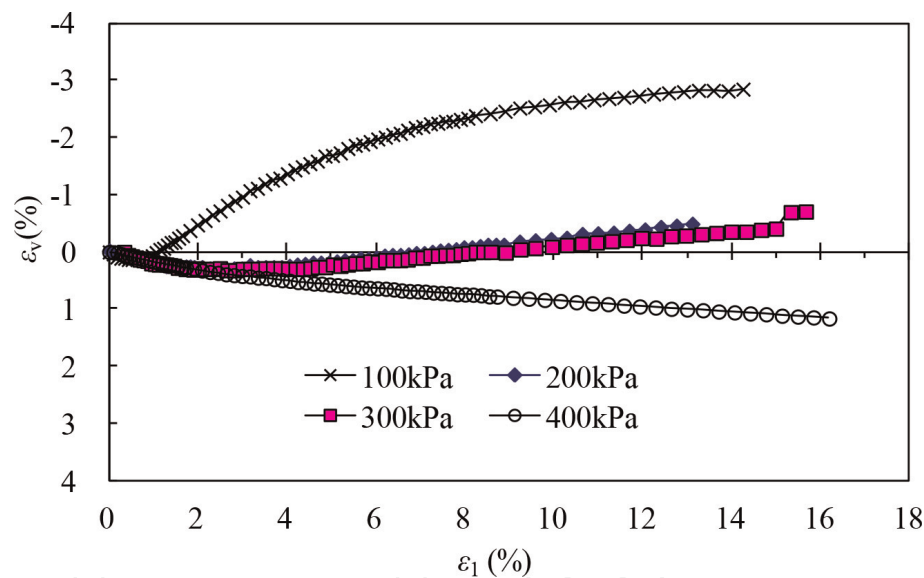
Figure 15.
Stress-strain curves.

Figure 16.
Curves of ε_v-ε_1.

be crushed, filled, and compacted under higher confining pressure. It was eventually manifested that the specimens transit gradually from strain softening status (e.g., when the initial confining pressure was 100 kPa) to strain hardening status (e.g., when the confining pressure was 200 kPa) with the increase of confining pressures on the samples. At any event, there exists a critical confining pressure. The samples soften in strain when the experiment confining pressures were lower than the critical confining pressures and harden in strain when the experimental confining pressures were higher than the critical confining pressures [18]. Thereafter, it could be deduced that the critical confining pressure in this study was between 100 and 200 kPa. It can be observed from **Figure 16** that the samples transit generally from shear dilation to shear shrinkage, and the volumetric strain of the transition point of the specimens increases gradually with the increase of confining pressures on the samples. In summary, as the confining pressure increases, the volumetric strain at failure changes toward volume contraction. According to

the results of large-scale triaxial tests, the Mohr's circles and the strength failure envelope can be depicted in **Figure 17** on the basis of the Mohr-Coulomb strength criterion. The linear Mohr's envelope of the weathered granite soil in this work can be expressed as

$$\tau_f = \sigma \, \tan 41.3° + 0.55 \text{ MPa}, \tag{5}$$

where τ_f is the peak shear stress and σ is the normal stress.

Eq. (5) shows that the cohesive strength of the samples is 55 kPa. However, because the weathered granite soil belongs to coarse grained soil, the cohesive strengths of the samples should be close to zero. It has been proved that the particles of coarse grained soil might be broken and its peak strength is nonlinear [19]. **Figure 18** shows that the ratio (τ_f/σ) is not constant but decreases when σ increases. In addition, the Mohr envelope is bending downward. The radius of bend reduces as the confining pressure increases, which reflects that the particle breakage is controlled by the confining pressures noticeably.

According to De-Mello [20], the power function of weathered granite soil in this study can be expressed as follows:

$$\tau_f = 0.361\sigma^{0.803} \tag{6}$$

As shown in **Figure 18**, the fitting envelope has a good correlation, which further explains that weathered granite soil has the property of nonlinear strength because of particle breakage. The nonlinear strength characteristics of compacted weathered granite soils could be affected by rock strength, intergranular friction, occlusal effect, etc. The mechanism of the nonlinear strength could be interpreted by means of the variation of failure surface angle in previous literature [21]. Under lower confining pressure, the internal friction angle was relatively large, the bending of the strength envelope was obvious, and the samples had the obvious characteristics of shear dilation and particle breakage. With the increase of confining pressure, the internal friction angle decreased and the bending degree of strength envelope decreased gradually. It was showed that under higher confining pressure, the strength characteristics of compacted weathered granite soils were mainly dominated by particle breakage.
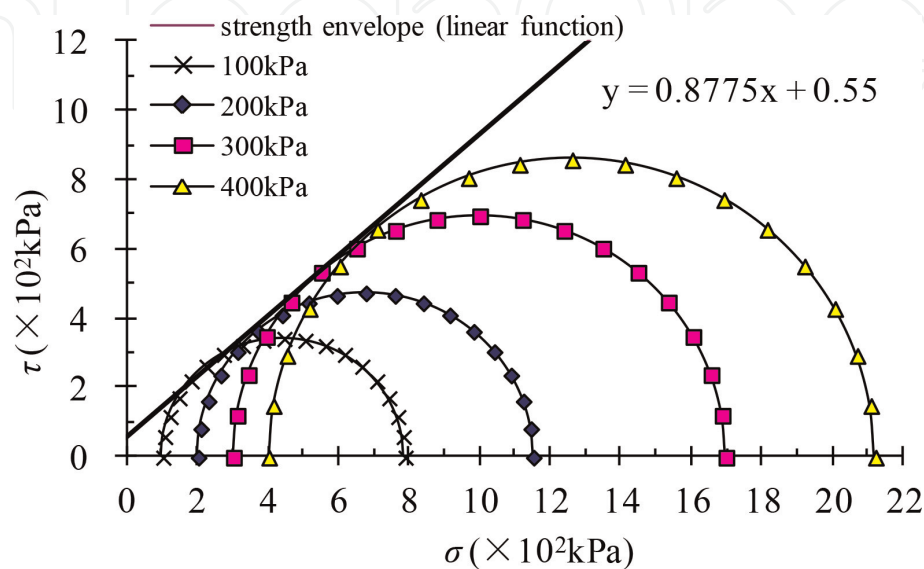

Figure 17.
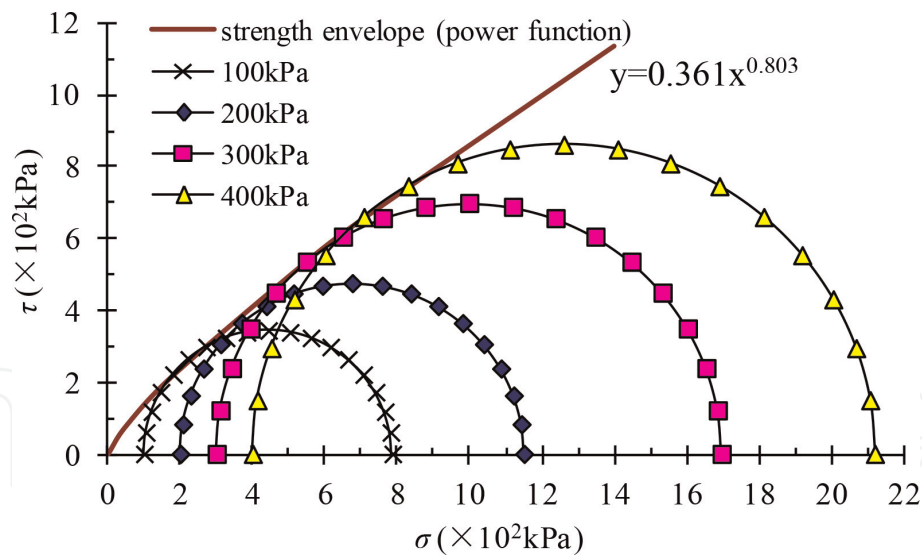*Mohr strength envelope of red-brown samples.*

Figure 18.
Actual strength envelope of red-brown samples.

5.4 Shearing-dilatancy characteristics

Weathered granite soil, as coarse grained soil, has obvious shear dilation property, which was found through the CD tests in this chapter. **Figure 19** shows the results of triaxial tests under difference confining pressures with respect to the relation between the stress ratio of q/p and the strain increment ratio of $d\varepsilon_v/d\varepsilon_1$. The tests were performed according to the stress and strain increment parameters used in widely accepted models, such as Cam-clay model, where $q = \sigma_1 - \sigma_3$ and $p = (\sigma_1 + 2\sigma_3)/3$. **Figure 19** shows the following observations: (1) under difference confining pressures, the strain increment ratio is always larger than zero at the initial point of shear. The ratio decreases with the increase of stress ratio q/p, which indicates that the volumetric strain of weathered granite soil changes toward the volume contraction. At the same time, the contraction ratio in the initial stage of triaxial shear is larger than that in the following stage. The reason for this
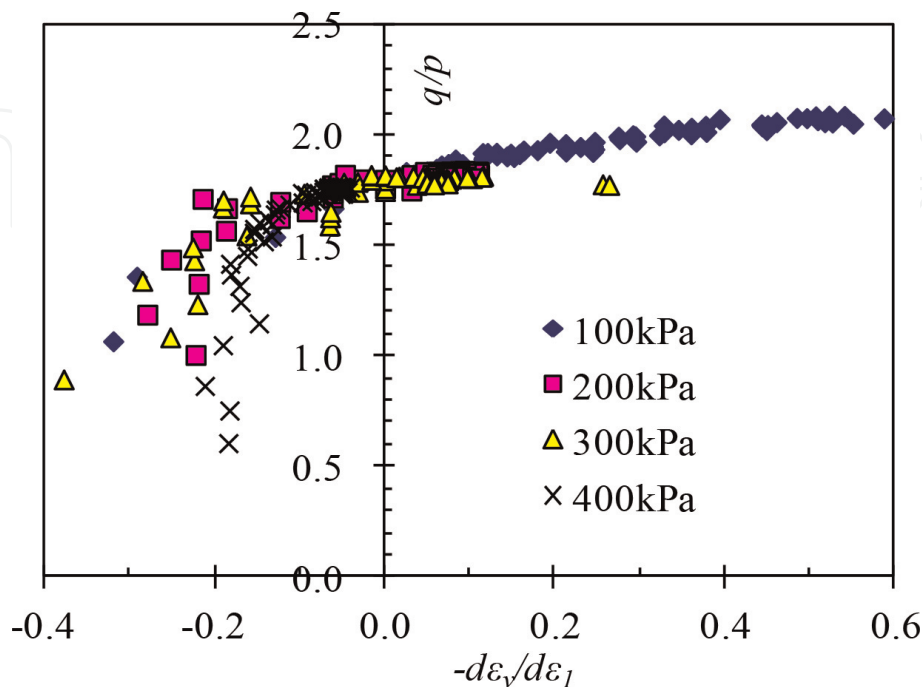

Figure 19.
q/p: $d\varepsilon_v/d\varepsilon_1$ of sample data with different confining pressures.

phenomenon is that once the soil reaches to a certain compaction rate, it gets difficult to compact further. (2) When the confining pressures change from 100 to 300 kPa, the strain increment ratio decreases as shear stress increases. The samples reached the stage transition point ($d\varepsilon_v = 0$) when the strain increment ratio was equal to zero at certain level of stress. After the stage transition point, with the increase of shear force, the $d\varepsilon_v/d\varepsilon_1$ ratio becomes negative. At this time, the volumetric strain of weathered granite soil changes toward volumetric contraction dilatancy. The aforementioned phenomena reflect the characteristics of dilatancy under lower confining pressures. The cause of the phenomena is due to the situation that the internal particles of weathered granite soil might be overturned and dislocated. (3) When the confining pressure is equal to 400 kPa, the $d\varepsilon_v/d\varepsilon_1$ ratio is always larger than zero during shearing processes. It indicates that interparticle contact stresses in the weathered granite soil increase gradually and the particle breakage becomes obvious under larger confining pressures. At this stage, the samples were made further denser as the broken particles filled into the voids of soil and the shrinkage behavior of soil samples is obvious.

Based on the above test results, there must exist a confining pressure between 300 and 400 kPa that makes the volumetric strain increment to be equal to zero. In other words, between the aforementioned observations (2) and (3), there must exist a relatively balanced state when the dilatancy caused by the overturn and dislocation of soil particles is equal to the shrinkage caused by the breakage and compaction of soil particles.

The curves of σ_1/σ_3 versus ε_v in **Figure 20** show the relationships between σ_1/σ_3 and ε_v. The relationships include two cases. One case is that the curve bends to left. The other case is that the curve bends to right. The volumetric strain of samples changes to the volume contraction initially and dilatancy later with the increase of the stress ratio of q/p under lower confining pressures, as shown in the former case when the curve bends to left. The volumetric strain of samples changes always toward the volume dilatancy with the increase of the stress ratio of q/p under larger confining pressures in the latter case when the curve bends to right.
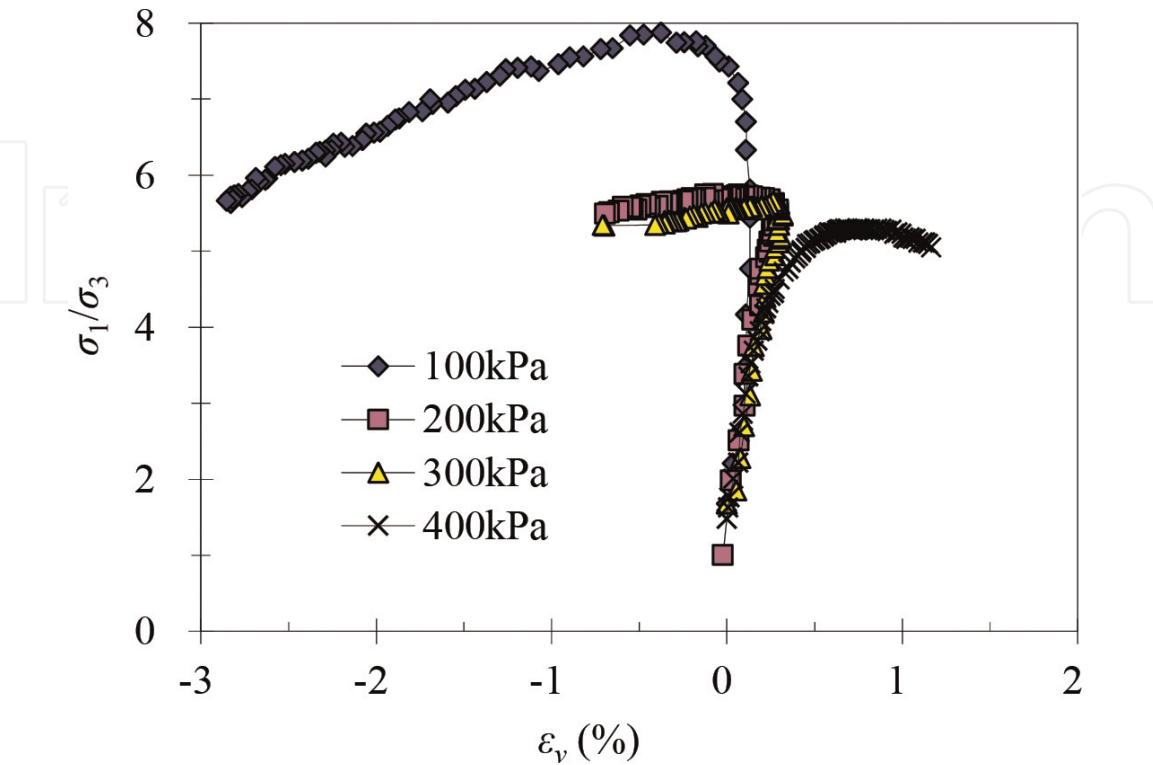

Figure 20.
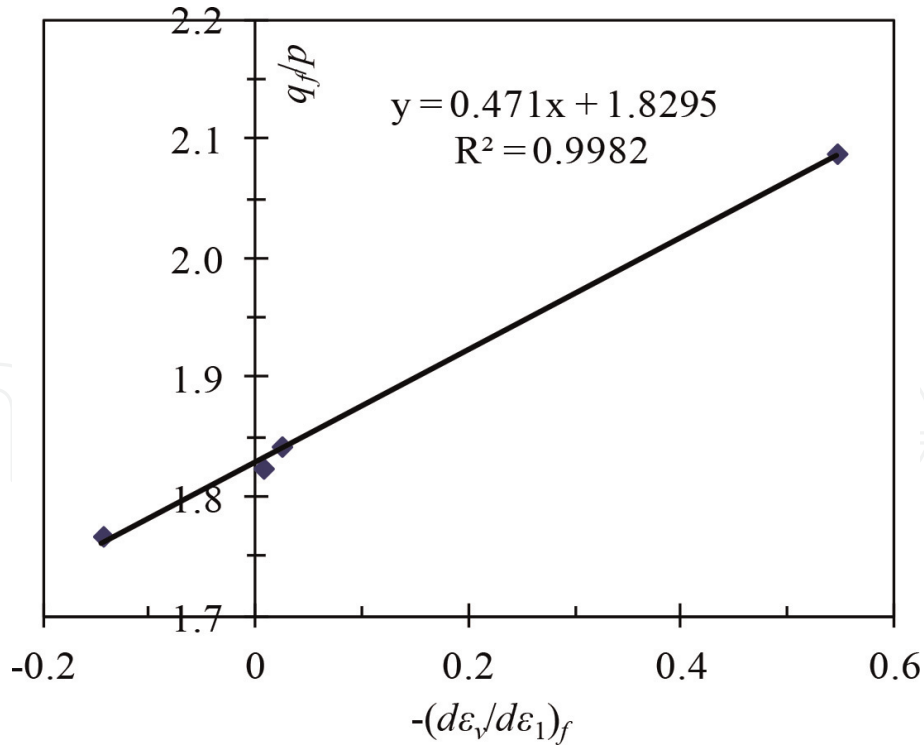*Curves of σ_1/σ_3 versus ε_v.*

Figure 21.
Curve of q_f/p versus $-(d\varepsilon_v/d\varepsilon_1)_f$.

Figure 21 shows the relationship between peak stress ratio and peak strain increment ratio. As shown in **Figure 21**, an approximate linear relationship can be found between q_f/p and $-(d\varepsilon_v/d\varepsilon_1)_f$. When the elastic deformation is neglected (i.e., $d\varepsilon_v/d\varepsilon_s = d\varepsilon_v^p/d\varepsilon_s^p$), M (q_f/p) is equal to 1.83 based on the stress-dilatancy equation in a Cam-clay model [22].

6. Constitutive model

6.1 Strength condition

Particle breakage occurs in general sand under higher confining pressure and in weathered granite soil under lower confining pressure [23]. According to the generalized nonlinear strength theory proposed by Yao et al. [24], M_f and M_c are expressed as follows [25, 26]:

$$M_f = M \left(\frac{p}{p_c} \right)^{-n},$$ (7)

$$M_c = M \left(\frac{p}{p_c} \right)^{n},$$ (8)

where M is the stress ratio at critical state, M_f is the stress ratio at shear failure, M_c is the stress ratio at characteristic state point, p_c is the reference breaking stress, and n is the material parameter. Substituting $M_f = q_f/p$ and $M_c = q_c/p$ into Eqs. (7) and (8), respectively, gets the function of q_f and q_c as Eqs. (9) and (10) on the p-q plane, which are the exponential functions:

$$q_f = M p_c^n p^{1-n},$$ (9)

$$q_c = M p_c^{-n} p^{1+n}. \tag{10}$$

It can be seen that the product of M_f and M_c is constant, as shown in Eq. (11).

$$M_f M_c = M^2, \tag{11}$$

The stress ratio at shear failure (M_f) and the stress ratio at characteristic state point (M_c) of granite weathered soil were calculated by a large-scale triaxial test under different confining pressures. **Figure 22** shows the shape of M_f and M_c in p-q plane. In this figure, M is the strength line determined by Mohr-Coulomb strength criterion and M_f is the actual peak strength line. From the figure, it is found that the Mohr-Coulomb strength of compacted weathered granite soil under lower confining pressure is smaller than that of the actual strength, while the strength of compacted weathered granite soil under higher confining pressure is higher than that of the actual strength. In other words, By using Mohr-Coulomb criterion, the strength of compacted weathered granite soil under lower confining pressure may be underestimated, while that of compacted weathered granite soil under higher confining pressure may be overestimated. The phenomenon of particle breakage has been found when the triaxial test for weathered granite soil in Ube, Japan, under 10–300 kPa confining pressure has been carried out by Miura et al. [23]. It can be considered that the inapplicability of the Mohr-Coulomb strength criterion for the weathered granite soil is caused by the particle breakage.

By fitting the stress ratio (M, M_f, and M_c) of weathered granite soil as shown in **Figure 9**, it is found that the expression by using Eqs. (12) and (13) is more accurate than by using Eqs. (7) and (8)

$$M_f = M \left(\frac{p}{p_c} \right)^{-4n}, \tag{12}$$
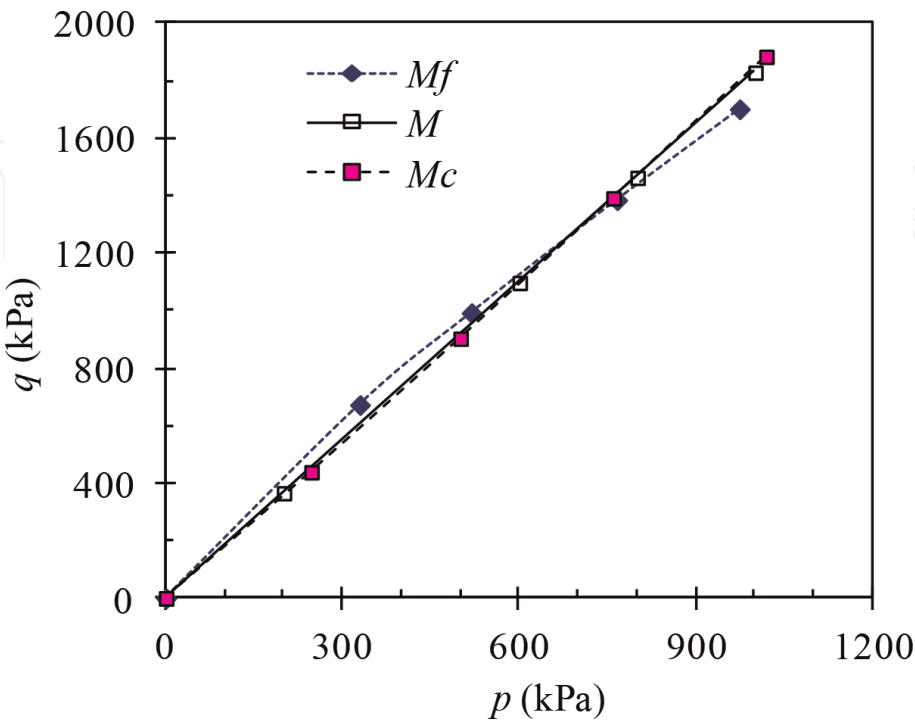
$$M_c = M \left(\frac{p}{p_c} \right)^{n}. \tag{13}$$

Figure 22.
Shape of M_f and M_c on p-q plane for samples.

17

According to Eq. (14),

$$M_f M_c = M^2 \left(\frac{p}{p_c} \right)^{-3n},$$ (14)

we can see that the product of M_f and M_c is not a constant, but a power function of p.

6.2 Constitutive model

6.2.1 Yield function

Based on the results of the isotropic consolidation test for Toyoura sand, Nakai [27] has established the relationship between the volumetric strain (including elastic volumetric strain and plastic volumetric strain) and the mean principal stress of sand,

$$\varepsilon_v^e = C_e \left[\left(\frac{p}{p_a} \right)^m - \left(\frac{p_0}{p_a} \right)^m \right],$$ (15)

$$\varepsilon_v^p = (C_t - C_e) \left[\left(\frac{p}{p_a} \right)^m - \left(\frac{p_0}{p_a} \right)^m \right],$$ (16)

where p_0 is the initial mean principal stress, p_a (=101.3 kPa) is the atmospheric pressure, m is a coefficient for sand, C_t is the compression index, and C_c is the swelling index. Based on the Eqs. (15) and (16), the yield function of weathered granite soil is constructed in this chapter.

When considering the particle breakage of soil, the stress-dilatancy equation in the modified Cambridge model was changed by Yao et al. [28] to the following form:

$$\frac{d\varepsilon_v^p}{d\varepsilon_s^p} = \frac{M_c^2 - \eta^2}{2\eta},$$ (17)

where ε_s^p is the plastic shear strain and η is q/p.
The orthogonality condition is

$$-\frac{d\varepsilon_v^p}{d\varepsilon_s^p} = \frac{dq}{dp},$$ (18)

The expression of the plastic potential function, which is obtained through the differential equation, composed of Eqs. (17) and (18), is expressed as

$$f = (2n + 1) \frac{p_c^{2n}}{M^2} \frac{q^2}{p} + p^{2n+1} - p_x^{2n+1} = 0.$$ (19)

According to Nakai's research [27], p_x is expressed as

$$p_x = \left(\frac{p_a^m}{C_t - C_e} \varepsilon_v^p + p_0^m \right)^{\frac{1}{m}}.$$ (20)

Substituting the Eq. (20) into the Eq. (19), we get

$$f = \frac{C_t - C_e}{p_a^m}\left\{\left[\frac{(2n+1)p_c^{2n}}{M^2}\frac{q^2}{p} + p^{2n+1}\right]^{\frac{m}{2n+1}} - p_0^m\right\} - \varepsilon_v^p = 0. \tag{21}$$

The above expression is the yield function of weathered granite soil. In the function, ε_v^p is an independent variable and can be used as the hardening parameter of the constitutive model of weathered granite soil.

6.2.2 Hardening parameter

On the basis of existing research results, Yao et al. [29] proposed the hardening parameters considering particle breakage as follows:

$$H = \int \frac{M_c^4\left(M_f^4 - \eta^4\right)}{M_f^4\left(M_c^4 - \eta^4\right)}\, d\varepsilon_v^p. \tag{22}$$

Simplifying the differential form of Eq. (21), we obtain

$$d\varepsilon_v^p = \frac{M_f^4\left(M_c^4 - \eta^4\right)}{M_c^4\left(M_f^4 - \eta^4\right)}\, dH. \tag{23}$$

Eq. (23) is used as a hardening parameter to construct the constitutive model of weathered granite soil.

6.2.3 Constitutive relation

By using the theory of plastic displacement potential and the associated flow rule and using the basic assumptions in the Cambridge model, after $d\varepsilon_v^p$ in the yield function, Eq. (21), was replaced by the hardening parameter H considering particle breakage in Eq. (22), we obtain,

$$\frac{\partial f}{\partial p} = \frac{C_t - C_e}{p_a^m} m\left[\frac{(2n+1)p_c^{2n}}{M^2}\frac{q^2}{p} + p^{2n+1}\right]^{\frac{m-2n-1}{2n+1}}\left(p^{2n} - \frac{p_c^{2n}}{M^2}\frac{q^2}{p^2}\right), \tag{24}$$

$$\frac{\partial f}{\partial q} = \frac{C_t - C_e}{p_a^m} m\left[\frac{(2n+1)p_c^{2n}}{M^2}\frac{q^2}{p} + p^{2n+1}\right]^{\frac{m-2n-1}{2n+1}}\left(\frac{2p_c^{2n}}{M^2}\frac{q}{p}\right), \tag{25}$$

$$\frac{\partial f}{\partial H} = -1 \tag{26}$$

According to the definition of generalized deviant stress, the plastic volumetric strain can be expressed as follows by means of a series of transformations of Eqs. (24)–(26):

$$d\varepsilon_v^p = \frac{m(C_t - C_e)}{p_a^m}\frac{M_f^4\left(M_c^4 - \eta^4\right)}{M_c^4\left(M_f^4 - \eta^4\right)}\left(dp + \frac{2\eta}{M_c^2 - \eta^2}\, dq\right)$$
$$\left[\frac{(2n+1)p^{2n+1}}{M_c^2}\eta^2 + p^{2n+1}\right]^{\frac{m-2n-1}{2n+1}}\left(p^{2n} - \frac{p^{2n}}{M_c^2}\eta^2\right). \tag{27}$$

The stress-dilatancy equation is expressed in the following form from Eqs. (17) and (27)

$$d\varepsilon_s^p = \frac{m(C_t - C_e)}{p_a^m} \frac{M_f^4}{M_c^4} \frac{(M_c^2 + \eta^2)2\eta}{(M_f^4 - \eta^4)} \left(dp + \frac{2\eta}{M_c^2 - \eta^2} dq \right) \cdot$$
$$\left[\frac{(2n+1)p^{2n+1}}{M_c^2} \eta^2 + p^{2n+1} \right]^{\frac{m-2n-1}{2n+1}} \left(p^{2n} - \frac{p^{2n}}{M_c^2} \eta^2 \right) \tag{28}$$

Equations (26) and (27) are the plastic strain expression of weathered granite soil considering particle breakage.

In three-dimensional axisymmetry, the following expressions can be obtained from the generalized Hook's law:

$$d\varepsilon_v^e = \frac{3(1 - 2v)}{E} dp \tag{29}$$

$$d\varepsilon_s^e = \frac{2(1 + v)}{3E} dp \tag{30}$$

where E is the elastic modulus and v is the Poisson's ratio.

After taking the derivative of p in Eq. (15), the elastic volumetric strain can be expressed as

$$d\varepsilon_v^e = \frac{mC_e p^{m-1}}{p_a^m} dp \tag{31}$$

Combining Eqs. (29)–(31), the elastic shear strain is obtained in the following form,

$$d\varepsilon_s^e = \frac{2(1 + v)mC_e p^{m-1}}{9(1 - 2v)p_a^m} dp \tag{32}$$

According to elastoplastic mechanics, the total volumetric strain and the total shear strain are, respectively, expressed as

$$d\varepsilon_v = d\varepsilon_v^e + d\varepsilon_v^p = \frac{m(C_t - C_e)}{p_a^m} \frac{M_f^4}{M_c^4} \frac{(M_c^4 - \eta^4)}{(M_f^4 - \eta^4)} \left(dp + \frac{2\eta}{M_c^2 - \eta^2} dq \right) \cdot$$
$$\left[\frac{(2n+1)p^{2n+1}}{M_c^2} \eta^2 + p^{2n+1} \right]^{\frac{m-2n-1}{2n+1}} \left(p^{2n} - \frac{p^{2n}}{M_c^2} \eta^2 \right) + \frac{mC_e p^{m-1}}{p_a^m} dp \tag{33}$$

$$d\varepsilon_s = d\varepsilon_s^e + d\varepsilon_s^p = \frac{m(C_t - C_e)}{p_a^m} \frac{M_f^4}{M_c^4} \frac{(M_c^2 + \eta^2)2\eta}{(M_f^4 - \eta^4)} \left(dp + \frac{2\eta}{M_c^2 - \eta^2} dq \right) \cdot$$
$$\left[\frac{(2n+1)p^{2n+1}}{M_c^2} \eta^2 + p^{2n+1} \right]^{\frac{m-2n-1}{2n+1}} \left(p^{2n} - \frac{p^{2n}}{M_c^2} \eta^2 \right) + \frac{2(1 + v)mC_e p^{m-1}}{9(1 - 2v)p_a^m} dq. \tag{34}$$

The Eqs. (33) and (34) are the constitutive relation of the weathered granite soils considering particle brakeage.

The seven parameters in the constitutive model of weathered granite soil are C_e, C_t, m, M, p_c, n, and ν. Except for Poisson's ratio ν, the other six parameters can be obtained by conventional triaxial test. The value of ν is assumed to be 0.3. C_e, C_t, and m can be obtained by isotropic compression and unloading test, and M, p_c, and n can be obtained by consolidated drained triaxial test.

7. Conclusions

In this chapter, routine physical and mechanics tests and large-scale triaxial tests were conducted to investigate the compaction, bearing, strength and shearing-dilatancy characteristics, and constitutive model of compacted weathered granite soil. The main conclusions obtained from the study in this chapter are summarized as below:

1. With an increase in burying depth of weathered granite, the geological year's parameter (m) decreases by power function, but the geometric progression constants (r) increase by power function. The exponent of power function in this chapter can be used to evaluate the weathering process of weathered granite [11].

2. The particle-breaking characteristics of weathered granite soils are obviously influenced by many factors such as particle gradation, mineral content, blows per layer, and stress level.

3. The pure weathered granite soil shows similar compaction characteristics of sands. The compression and bearing characteristics of weathered granite soil vary significantly when the clay content ratio changes. The weathered granite soil in this chapter can be used as the filling material.

4. The experimental results show that the increase in peak deviatoric stress q_f due to an increase in mean stress p is observed as nonlinear under lower confining pressure because of the existence of particle breakage. It is found that the product of the state stress ratio and peak stress ratio is not a constant but a power function of an average main stress. The research results are helpful to understand the law of the long-term degradation of subgrade performance due to particle breakage of weathered granite soil.

Given that wet conditions may influence the evolution of embankments after construction, future extensive research should be focused on dynamic measurement methods of particle breakage and long-term behavior degradation analysis of subgrade as a result of further weathering and particle breakage [7, 11, 30, 31]. It is very difficult to entirely understand the road performance of weathered granite soil due to its special mechanical properties. Further research needs to be performed for assessing the unique mechanical behaviors of compacted weathered granite soil considering particle breakage and the mechanical properties of different types of weathered granites soils (e.g., coarse-grained weathered granite soil and fine-grained weathered granite soil). Given that measuring particle breakage and its variations during triaxial compression tests are still a challenging task [32], future extensive research should be focused on the dynamic measurement methods, the mathematical description of particle breakage, and the long-term behavior degradation owning to particle breakage [33].

Acknowledgements

Conflict of interest

The authors declare no conflict of interests.

Author details

Xirong Niu
Department of Civil Engineering, Shanxi University, Taiyuan, Shanxi, China

*Address all correspondence to: niuxirong@sxu.edu.cn

IntechOpen

References

[1] Lu F, Sang L. Petrology. Beijing: Geological Publishing House; 2002. p. 120

[2] Wu N, Zhao C, Hou W. Research on the cause of formation, distribution and engineering characteristics of the granite residual soil. Journal of Pingdingshan Institute of Technology. 2004;**13**:1-4

[3] Writing Committee of Handbook of Engineering Geology (WCHEG). Handbook of Engineering Geology. 4th ed. Beijing: China Building Industries Press; 2007. p. 125

[4] Fukumoto T. A grading equation for decomposed granite soil. Soils and Foundations. 1990;**30**:27-34. DOI: 10.3208/sandf1972.30.27

[5] Yu F. Particle breakage and the drained shear behavior of sands. International Journal of Geomechanics. 2017;**17**:04017041. DOI: 10.1061/(ASCE)GM.1943–5622.0000919

[6] Niu X, Yao Y, Chen Z. The strength and constitutive model of compacted weathered granite soils in Lüliang mountains. Rock and Soil Mechanics. 2017;**38**:2833-2840. DOI: 10.16285/j.rsm.2017.10.008

[7] Konrad JM, Salami Y. Particle breakage in granular materials—A conceptual framework. Canadian Geotechnical Journal. 2018;**55**:710-719. DOI: 10.1139/cgj-2017-0224

[8] Ministry of Transportation of the People's Republic of China (MOTPRC) Test Methods of Soil for Highway Engineering (JTG E40-2007). Beijing: People's Communications Press; 2007

[9] China Electronics Corporation (CEC). Code for Coarse-Grained Soil Tests for Hydropower and Water Conservancy Engineering (DL/T 5356-2006). Beijing: China Power Press; 2006

[10] Geng Y, Yang C, Song B, Wan Y. Post-orogenic granites with an age of 1800 ma in Luliang area, North China Craton: Constraints from isotopic geochronology and geochemistry. Geological Journal of China Universities. 2004;**10**(4):477-487. DOI: 10.3969/j.issn.1006-7493.2004.04.001

[11] Niu X, Yao Y, Sun Y, Luo Z. Weathering process of in situ granite and particle breakage characteristics of compacted weathered granite. Applied Sciences. 2018;**87**:1108. DOI: 10.3390/app8071108

[12] Hardin BO. Crushing of soil particles. Journal of Geotechnical Engineering. 1985;**111**:1177-1192. DOI: 10.1061/(ASCE)0733-9410(1985)111:10(1177)

[13] Leslie DD. Large scale triaxial tests on gravelly soils. In: Proceedings of the 2nd Pan-American Conference on Soil Mechanics and Foundation Engineering; 16-24 July 1963; Rio de Janeiro, Brazil. Vol. 1. São Paulo, Brazil: Associacao Brasileira de Mecanica dos Solos; 1963. pp. 181-202

[14] Leslie DD. Shear Strength of Rockfill, Physical Properties. Sausalito, CA, USA: Engineering Study No. 526; South Pacific Division, Corps of Engineers Laboratory; 1975. p. 124

[15] Marsal RJ. Discussion of shear strength. In: Proceedings of the 6th International Conference on Soil Mechanics and Foundation Engineering; Montreal, QC, Canada. Vol. 3. 1965. pp. 310-316

[16] Lee KL, Farhoomand I. Compressibility and crushing of granular soils in anisotropic triaxial compression. Canadian Geotechnical Journal. 1967;**4**:68-86. DOI: 10.1139/t67-012

[17] Niu X, Sun Y, Yao Y, Han J. Basic properties and weathering process of

strong weathered granite. Japanese
Geotechnical Society Special
Publication. 2015;**1**:8-33. DOI: 10.3208/
jgssp.CPN-07

[18] Lee IK, Coop MR. The intrinsic
behaviour of a decomposed granite soil.
Geotechnique. 1995;**45**:117-130. DOI:
10.1680/geot.1995.45.1.117

[19] Liu M, Gao Y, Liu H, Chen Y. Large-
scale triaxial test study on deformation
and strength characteristics of rockfill
materials. Chinese Journal of Rock
Mechanics and Engineering. 2003;**22**:
1104-1111. DOI: 10.3321/j.issn:
1000-6915.2003.07.011

[20] De-Mello VFB. Reflections on
decisions of practical significance to
embankment dam construction.
Géotechnique. 1977;**27**:281-355. DOI:
10.1680/geot.1977.27.3.281

[21] Vesic AS, Clough GW. Behavior of
granular materials under high stresses.
Journal of the Soil Mechanics and
Foundations Division. 1968;**94**:661-688

[22] Roscoe KH, Burland JB. On the
generalized stress-strain behavior of
"wet" clay. In: Engineering Plasticity.
Cambridge, U.K.: Cambridge Univ.
Press; 1968. pp. 535-609

[23] Miura N, O-Hara S. Particle-
crushing of a decomposed granite soil
under shear stresses. Soils and
Foundations. 1979;**19**:1-14. DOI:
10.3208/sandf1972.19.3_1

[24] Yao Y, Lu D, Zhou A. Generalized
non-liner strength theory and its
transformed stress space. Science in
China, Series E Technological Sciences.
2004;**47**:691-709. DOI: 10.1360/
04ye0199

[25] Yao Y, Zhou A, Lu D. Extended
transformed stress space for
geomaterials and its application. Journal
of Engineering Mechanics. 2007;**133**:
1115-1123. DOI: 10.1061/(asce)
0733-9399(2007)133:10(1115)

[26] Yao Y, Sun D, Matsuoka H. A
unified constitutive model for both clay
and sand with hardening parameter
independent on stress path. Computers
and Geotechnics. 2008;**35**:210-222. DOI:
10.1016/j.compgeo.2007.04.003

[27] Nakai T. An isotropic hardening
elastoplastic model for sand considering.
Soils and Foundations. 1989;**29**:119-137

[28] Yao Y, Matsuoka H, Sun D. A unified
elastoplastic model for clay and sand with
the SMP criterion. In: Proceedings of the
8th Australia-New Zealand Conference
on Geomechanics; Hobart, Australia.
Hobart: Australian Geomechanics
Society; 1999. pp. 997-1003

[29] Yao Y, Sun D, Luo T, Matsuoka H. A
simple 3-D constitutive model for both
clay and sand. Chinese Journal of
Geotechnical Engineering. 2002;**24**:
240-246. DOI: 10.3321/j.issn:
1000-4548.2002.02.026

[30] Wang W, Coop MR. An
investigation of breakage behaviour of
single sand particles using a high-speed
microscope camera. Géotechnique. 2016;
66:1-15. DOI: 10.1680/jgeot.15.P.247

[31] Niu X, Xie H, Sun Y, Yao Y. Basic
physical properties and mechanical
behavior of compacted weathered
granite soils. International Journal of
Geomechanics. 2017;**17**:04017082. DOI:
10.1061/(ASCE)GM.1943-5622.0000983

[32] Indraratna B, Thakur PK, Vinod JS,
Salim W. Semiempirical cyclic
densification model for ballast
incorporating particle breakage.
International Journal of Geomechanics.
2012;**12**:260-271. DOI: 10.1061/(ASCE)
GM.1943-5622 .0000135

[33] Chazallon C, Hornych P, Mouhoubi
S. Elastoplastic model for the long-term
behavior modeling of unbound granular
materials in flexible pavements.
International Journal of Geomechanics.
2006;**6**:279289. DOI: 10.1061/(asce)
1532-3641(2006)6:4(279)